Improve the Hot Corrosion Behaviors of the Inconel 738LC Coating with Nano YSZ–CNTs

Kadhim F. Alsultani[1,*], Hassan Sh. Majidi[2], and Sara Abdulameer[3]

[1]Universty of Babylon, Babylon, Iraq
[2]Al-Mustaqbal University College, Babylon, Iraq
[3]Iraqi Ministry of Education, Iraq
Email: finteelalsultani@gmail.com (K.F.A.), hasanshker@icoud.com (H.S.A.), Sara966@yahoo.com (S.A)
[*]Corresponding author
Manuscript received August 8, 2023; revised September 10, 2023; accepted October 3, 2023

***Abstract*—In this work, Inconel 738LC is coated with coatings with nano Yttria Stabilized Zirconia (YSZ) with different percentages of Carbon Nano Tubes (CNTs) which were done by using the technique of the plasma thermal spray. YSZ coating with different percentages of CNTs (100% nano YSZ, 96% nano YSZ + 4% CNTs, 94% nano YSZ + 6% CNTs, and 92% nano YSZ + 8% CNTs), adopting the plasma spray technique. The behavior of the Inconel 738LC alloy with and without artificial ash (67% wt. H_2SO_4 and 33% wt. V_2O_5) at different temperatures (650 ºC, 750 ºC, 850 ºC, and 950 ºC) was investigated. The cycles of hot corrosion and oxidation were achieved in an electric furnace for 10 cycles of 5 h each. At the completion of each cycle, the weight changes were measured and recorded. The Search Engine Marketing (SEM) and X-RayDiffraction (XRD) achieved for all the specimens were noted, prior and post the corrosion.**

***Keywords*—Inconel 738LC, oxidation, hot corrosion, Yttria Stabilized Zirconia (YSZ)–Carbon Nano Tubes (CNTs), artificial ash**

I. Introduction

Gas power plants in Iraq represent an important resource of electrical energy. To ensure the highest performance and efficiency in these plants, numerous components and units must, of necessity, correctly work together. The gas turbine is the principal unit, the very heart as it were, containing a large variety of highly advanced materials called superalloys, which can resist extreme thermal and chemical environments [1]. The nickel-based superalloys display Face-Centered Cubic (FCC) solid solutions (γ) with sufficient quantities of Al and Ti, in order to produce the Ni3(Ti, Al), fcc γ' precipitate, and M23C6/M6C carbides that are present at the grain boundaries [2, 3].

Turbine blade failure actually stops the turbines from working, producing a power plant outage that can stretch from one to four weeks or even longer at times, depending upon the amount of damage done and the technique adopted to restore the machine back to normal running, all causing severe financial losses [4]. A few of the causes that lead to failure, either rapidly or slowly, are the hot exhaust gases, high pressure, high speed and the presence of heavy fuel contaminants. The most dominant reasons for failure induced by the high temperatures and presence of dangerous pollutants include Hot Corrosion (HC) and erosion corrosion [5]. For hot corrosion to occur no electrolyte environment is required; it takes place because of the deposition of impurities and salts like sodium sulfate and vanadium oxides [6] Sodium sulfate (Na_2SO_4) ranks among the common categories that play a direct part in the corrosion of molten salt, and is produced through the interaction between sulfur and sodium chloride during the process of burning the fuel oils. Both species were found present as contaminants in the burning air and fuel. Vanadium, an impurity present in fuel oil, can cause huge corrosion problems due to the formalization of V_2O_5, the melting point of which is 670 °C [7–9]. High temperature coatings can raise the corrosion resistance of the Ni-based superalloys. Hence, the NiBSs find extensive use in gas turbine blades [10, 11]. In fact, TBC is a kind of ceramic coating that is spread onto the constituents or elements that comprise a system to ensure the highest protection possible, against the most intense and extreme operating temperatures. A TBC, therefore, is composed of a metal bond coat, metal substrate, and a ceramic top coat. Under harsh and severely intense settings of working conditions, the intermediate bond coat (MCrAlY) plays a pivotal part in the adherence of the ceramic top coat and thus raises the resistance to attack, normally induced by the molten salt and oxygen [12–14].

As they are well known for their remarkable mechanical properties, CNTs are widely used to create aluminum-based composites; the CNTs have been found to function as bridges across the voids and cracks, and are distributed uniformly in the aluminum matrix [15].

Due to these good qualities the coatings are deposited via the plasma spraying technique onto most materials that act as the substrate, and which possess a similar melting point, such as metal alloys, ceramics, and cermet. Indeed, the TBCs sprayed with plasma have low thermal conductivity values and exceptional chemical stability, even when the temperatures increase to high levels [16–18].

II. Experimental Work

Specimens were collected by cutting the turbine blade represented Inconel 738LC to the specific dimensions of 20×15×3.5 mm of length, width and thickness, respectively. Once these specimens were cut, they were ground with SiC grinding papers. Next, alumina paste was used to polish them, and making the chemical composition for the specimens, as shown in Table 1. As displayed in Table II, the specimens were coated with an intermediate coating layer termed the bond layer, and the thickness layer 150… Next, the specimens were coated with an outer ceramic layer made nano Yttria Stabilized Zirconia (YSZ) up of having different weight percentages from the Carbon Nano Tubes (CNTs).

doi: 10.18178/ijcea.2024.15.1.806

Table 1. Chemical composition for Inconel 738LC specimens

Elements	Wt. (%)
Ti	3.2
Cr	15.7
Fe	0.07
Co	8.1
Nb	0.8
Mo	1.8
Ta	1.5
W	2.5
Ni	Bal
LEC	3.4

The plasma spraying technique involved the use of a special of spraying unit (semi-automated), and the coating was accomplished by atmospheric plasma; the coating materials were combined in a ball mill once the bond layer coating was sprayed on the specimens whose surfaces were prepared prior to this step.

The fuel contaminations were prepared by mixing 67% wt. of Na_2SO_4 and V_2O_5. The hot corrosion weight change tests were then performed at (650 ºC, 750 ºC, 850 ºC, and 950 ºC, respectively), prior to and post coating the specimens with the contamination, by ash (67% wt. Na_2SO_4 and 33% wt. V_2O_5).

Table 2. Chemical composition of bond layer

Elements	Wt. (%)
Ni	3.2
Cr	21
Al	18
Y	0.5
Co	Bal

III. Results and Discussions

From Fig. 1 the SEM of the coated specimens are shown; with 100% YSZ (A), 96% wt. YSZ-4% wt. CNTs (B), 94% wt. YSZ-6% wt. CNTs (C) and 92% wt; YSZ-8% wt. CNTs (D); These images show that the coating layers are relatively high in porosity; the different coating layers show differences based on the degree of porosity.

Microcracks may be present, initiated by the thermal stresses produced during coating process. When porosity and microcracks are present, they prove to be detrimental to the coating properties. The SEM micrographs clearly showed partially melted and unmelted particles or particle clusters, in almost all the coating layers.

Agglomeration of the CNT particles or other particles in nanoscale may be the cause for the poor or partial melting.

Voids may be produced during the plasma spray process, as indicated through the SEM images. These voids result from a sequence of the plasma torch moving back and forth. They may be highly detrimental to the corrosion protection behavior as they could open a path for the passage of oxygen into the substrate. This action was used to analyze the SEM images, and thus assess the porosity percentage of the coating layer.

During the plasma spraying process, the pores and micro-cracks can arise from a variety of sources, for instance, the entrapped gases, incomplete filling in the splats which showed quick solidification, and the shrinking of the splats during the latter process, and so on. The porosity of the plasma sprayed coatings can range from below 2% to an excess of 20%, depending on the coating process parameters, as well as the properties of the coating powders utilized.

Specimens coated with 96% wt. YSZ-4% wt. CNTs (B), YSZ-6% wt. CNTs(C), and 92% wt. YSZ-8% wt. CNTs (D), possess a relatively lesser degree of porosity. The splats are smaller in size, and irregular in shape. These images indicate that the coatings have displayed lesser degree of porosity, as well as fewer microcracks.

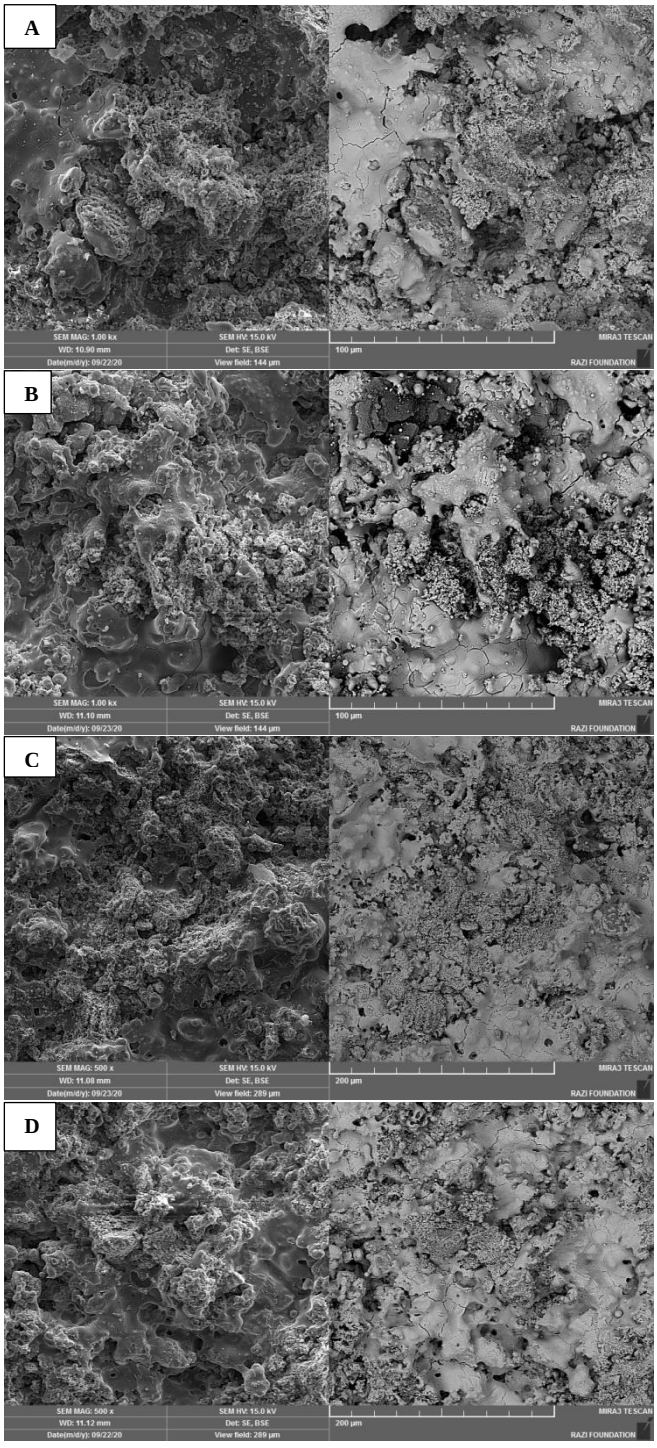

Fig. 1. SEM showed that the specimens coated with 100% wt.YSZ (A), 96% wt. YSZ-4% wt. CNTs (B), 94% YSZ-6% wt. CNTs (C), and 92% wt. YSZ -8% wt. CNTs (D).

From Fig. 2 the weight change per unit surface area is evident as a function of time, and expressed in the number of cycles for the bare specimens. The curve shows clearly that the maximum weight gain occurs at 950 ℃, which is possibly due to the high oxidation rate at this temperature. With the

increase in time, the thickness of the oxide layer also increased, i.e., the stresses in the layer increased because of the cracks and voids that were present.

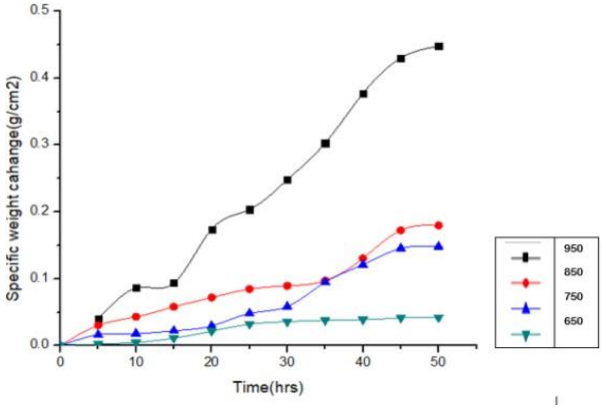

Fig. 2. Bare base alloy oxidation behavior at 950 ℃ temperature at different times.

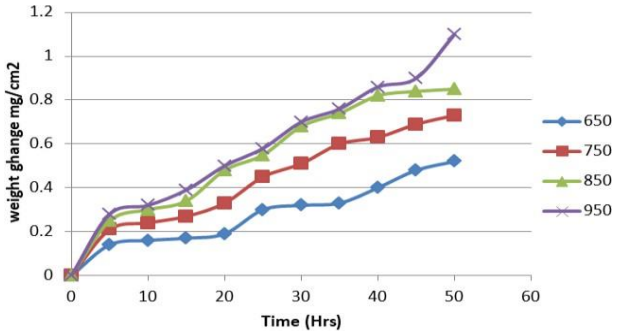

Fig. 3. The relation between weight change and different temperatures at the present artificial ash, after 50 h for coated.

In Fig. 4 the XRD results of the specimens exposed to oxidation reveal that at 650 ℃, 750 ℃, 850 ℃ and 950 ℃ for 50 h, are listed. The oxides formed include NiO, TiO_2, and spinel phase $NiCr_2O_4$. All these oxide types are the pores which do not adhere very well to the base metal surface, and hence they are not the protective oxide layer. The Cr_2O_3 which was visible at the interface between and the alloy matrix was a layer abundant in nickel oxide. When the Cr_2O_3 sub-layer was continuous, an outer NiO scale was formed, with an interior layer, which sometimes appeared porous in nature, composed of NiO, and included the $NiCr_2O_4$ islands. The Nio layer stopped developing and the kinetics of oxidation barely displayed the growth of the Cr_2O_3 layer. When the spinel $NiCr_2O_4$ was introduced into the external layer, it caused a chemical reaction between the Cr_2O_3 and NiO layers. Some $NiCr_2O_4$ was produced by the oxygen moving ahead of the NiO front. In all the Cr alloys, (except for the most dilute ones) these $NiCr_2O_4$ islands continued to remain as a second phase in the scale, and their degree revealed the site of the original metal surface. Hot corrosion test performed was based on the change in weight; test results were obtained at different times with different temperatures; weight change is a good indicator to study the corrosion rates under equivalent conditions.

Change in weight is measured per the corresponding time cycle. Fig. 3 indicates the hot corrosion behavior (weight change) in artificial ash having a composition of 67% wt. V_2O_5 and 33% wt. Na_2SO_4 at 650 ℃, 750 ℃, 850 ℃, and 950 ℃.

At 950 ℃, the specimen displayed much higher rates of weight gain, which continued until the last cycle. The weight change at 650 ℃ showed that the specimen had reduced drastically in comparison with the other temperature. The change in weight observed in the specimens, in presence of artificial ash, had increased, when compared with those of oxidation, without artificial ash salts.

Fig. 5 appear many primary peaks $(ZrO)_2$ in all the tested samples results, in addition to appearing $(ZrO)_2$ (m) and $(YVO)_4$. The reaction between sodium vanadate $(NaVO)_3$ and yittrium oxide (Y_2O_3) produces yttrium vanadate $((YVO)_4)$ and leads to the transformation of tetragonal zirconia to monoclinic zirconia. These results are in agreement with results reported by other researchers [19, 20].

Different forms of carbon (diamond and graphite) were found in some rested specimens. The CNTs reinforced coatings enhance resistance to corrosion significantly [21].

Sodium oxide was also noticed in XRD patterns in many phases; Na_2S2O_3, Na_2SO_4, and $Na_2S_2O_4$. It presented as an outer layer of the specimens that covered with prior to corrosion test. Other phases and elements may present in a small amounts and these amounts cannot be detected by XRD. Absence of any oxides of base specimen's results implies that the coating layer was successful to isolate the substrate from the surrounded corrosive environment.

Furthermore, after HC test, the results of XRD revealed that no reaction product of Na_2SO_4 with $(ZrO)_2$ could be observed. As a result, Na_2SO_4 had no influence on the YSZ coating. It appears that the molten $(NaVO)_3$ simply improved mobility of atom and accelerated (enhanced) yttria depletion. Other researchers have corroborated this behavior as well.

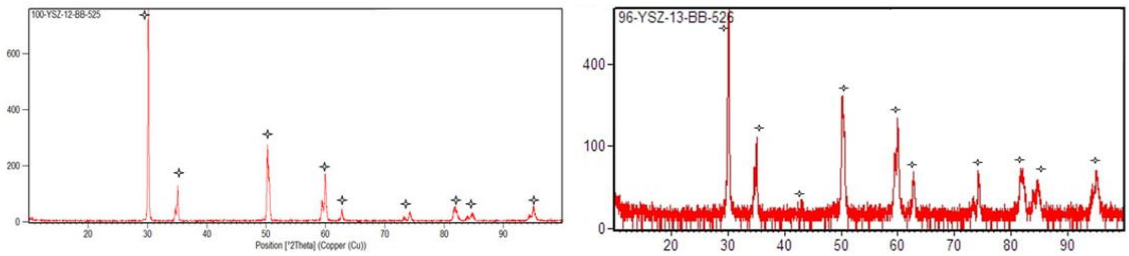

(A) (B)

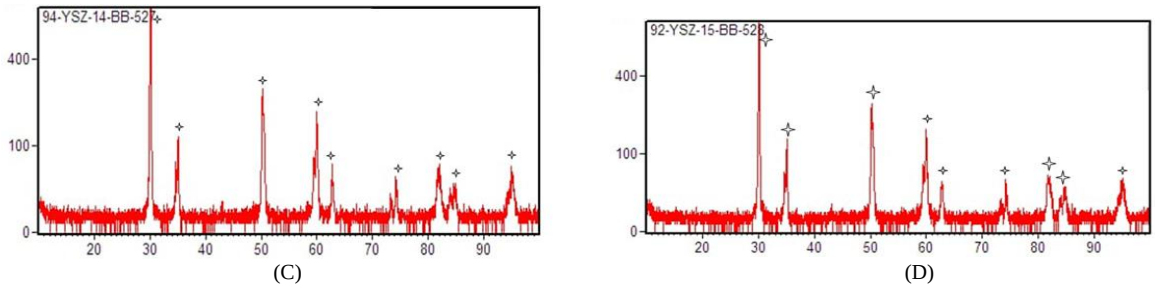

(C) (D)

Fig. 4. XRD patterns for specimens, 100% wt. YSZ (A), 96% wt. YSZ– 4% wt. CNTs (B), 94% YSZ- 6% wt. CNTs (C), and 92% wt. YSZ – 8% wt. CNTs (D) at 850 ºC after 50 hours oxidation.

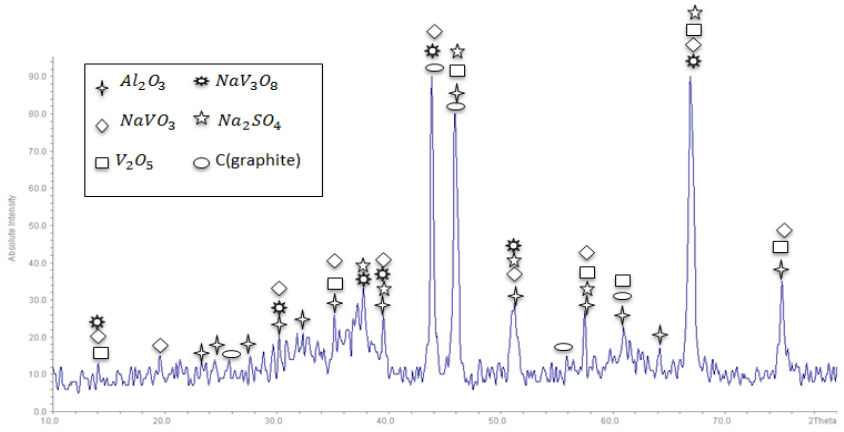

(A)

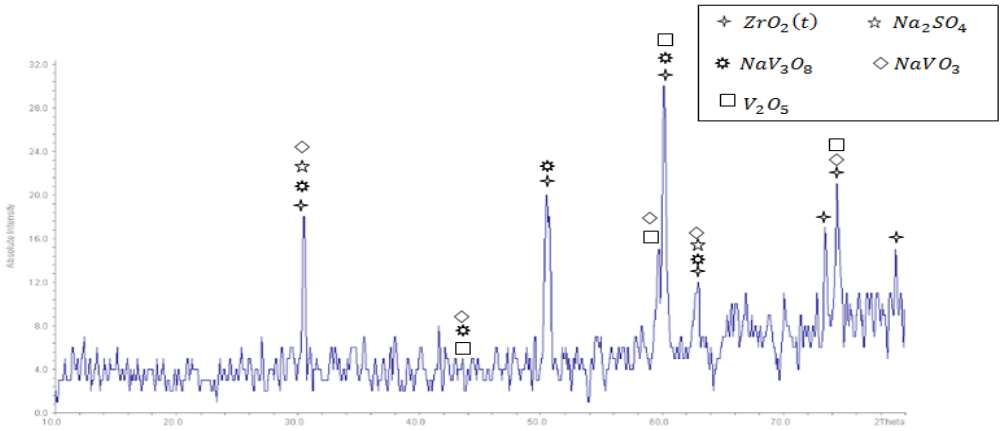

(B)

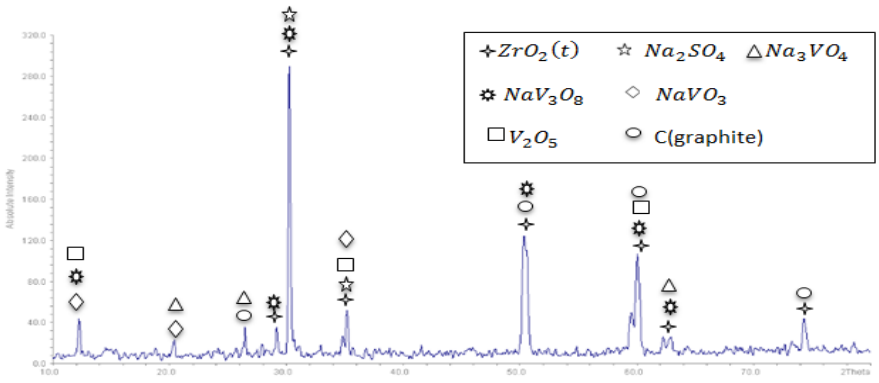

(C)

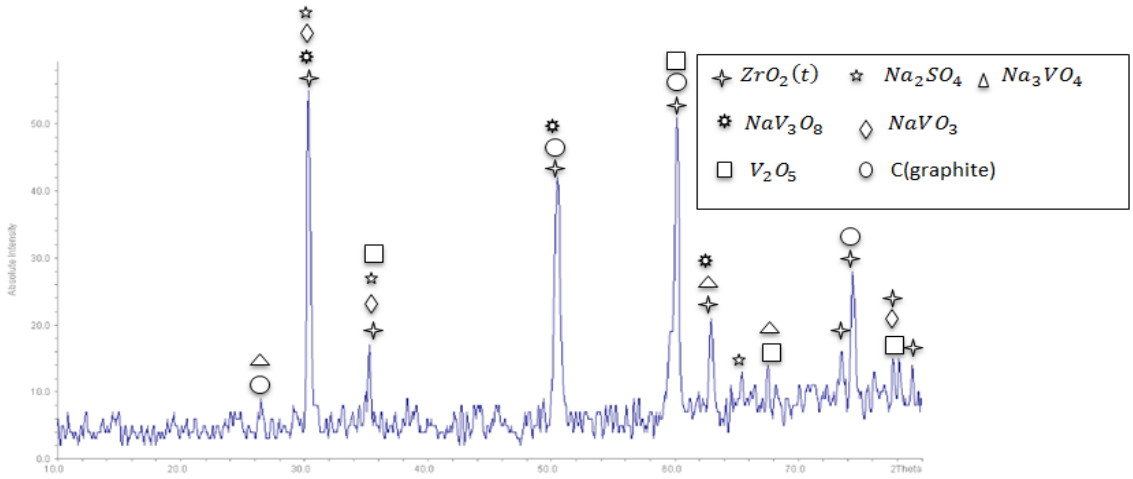

(D)

Fig. 5. XRD patterns of the specimens coated with 100% wt. YSZ (A), 96% wt. YSZ-4% wt. CNTs (B), 94% YSZ-6% wt. CNTs (C), and 92% wt. YSZ-8% wt. CNTs (D) with h test at 950 °C.

IV. Conclusions

Hot corrosion and oxidation rates of bare specimens increase with time and temperature as the oxide layer increase, becoming porous and weakly adhering to the substrate's surface. The greatest weight change take place at 950 °C and 50 h. The results of XRD reveals the presence of oxides of Ni, Cr, and Ti and spinal phases $NiCr_2O_4$ and $Ni(VO_3)_2$ The micrographs SEM results showed that the surface layer that formed during corrosion is porous and cracked. All layers of coatings exhibit good hot corrosion resistance compared with uncoated specimen and less change in weight than that corresponding in the bare specimen. The addition of CNTs enhances the properties of the coating layer, such as porosity and voids are decreased. XRD results of coated specimens after hot corrosion indicate that no any oxide if base specimen this imply that the layer of coating was succeed to separate the substrate from the external and harm corrosive environment.

Conflict of Interest

The authors declare no conflict of interest.

Author Contributions

Sara Abdulameer conducted the research under the supervision of both Kadhim F. Alsultani and Hassan Sh. Majidi. All authors approved the final version.

References

[1] B. Geddes, H. Leon, and X. Huang, "Superalloys: Alloying and performance," *ASM International*, 2010.

[2] M. Amin, "Oxidation behaviour of IN-738 LC superalloys in the presence of ionic salts at 1173 K," *Portugaliae Electrochimica Acta*, vol. 21, no. 4, pp. 389–398, 2003.

[3] B. Sami and M. Husain, "Effect of electro-spark deposition process on surface properties for gas turbine blades," Doctoral dissertation, Thesis the University of Technology, 2013.

[4] S. Rani, "Common failures in gas turbine blade: A critical review," *Int. J. Eng. Sci. Res. Technol*, vol. 3, pp. 799–803, 2018.

[5] Roberge and R. Pierre, *Handbook of Corrosion Engineering*, McGraw-Hill Education, 2000, vol. 1, pp. 222–265.

[6] F. Y. Najy, K. F. Al-Sultani, and J. M. A. Murshdy, "Study addition double inhibitor consist of MgO and SiO_2 to residual oil to prevent hot corrosion of stainless steel (304 L) of boilers pipes in power generation station," *Advances in Natural and Applied Sciences*, vol. 11, no. 2, pp. 57–68, 2017.

[7] J. Porcayo-Calderon, V. M. S. Bravo, R. A. Rodriguez-Diaz, and L. Martinez-Gomez, "Effect of the $NaVO_3$-V_2O_5 ratio on the high temperature corrosion of chromium," *Int. J. Electrochem. Sci*, vol. 10, pp. 4928–4945, 2015.

[8] R. A. Rapp, "Chemistry and electrochemistry of hot corrosion of metals," *Materials Science and Engineering*, vol. 87, pp. 319–327, 1987.

[9] L. Bansal, V. K. Rathi, and K. Mudafale, "A review on gas turbine blade failure and preventive techniques," *Int. J. Eng. Res. Gen. Sci*., vol. 6, pp. 54–62, 2018.

[10] Boyraz and M. Tarık, "IN 738 LC microstructure optimization with heat treatment and simulation to improve mechanical properties of turbine blades," MSc dissertation, The Graduate school of Natural and Applied Sciences, Middle East Technical University, 2018.

[11] M. Shourgeshty, M. Aliofkhazraei, and M. M. Alipour, "Introduction to high-temperature coatings," *High Temperature Corrosion*. *InTech*, 2016. http://dx.doi.org/10.5772/64282

[12] Z. Xu, Z. Wang, G. Huang, R. Mu, and L. He. "Morphology, bond strength and thermal cycling behavior of (Ni, Pt) Al/YSZ EB-PVD thermal barrier coatings," *Journal of Alloys and Compounds*, vol. 651, pp. 445–453, 2015.

[13] P. Mohan, T. Patterson, V. H. Desai, and Y. H. Sohn "Degradation of free-standing air plasma sprayed CoNiCrAlY coatings by vanadium and phosphorus pentoxides," *Surface and Coatings Technology*, vol. 203, no. 5–7, pp. 427–431, 2008.

[14] G. D. Girolamo, M. Alfano, L. Pagnotta, A. Taurino, J. Zekonyte, and R. J. K. Wood, "On the early stage isothermal oxidation of APS CoNiCrAlY coatings," *Journal of Materials Engineering and Performance*, vol. 21, no. 9, pp. 1989–1997, 2012.

[15] L. Wang, Y. Wang, X. G. Sun, J. Q. He, Z. Y. Pan, and C. H. Wang, "Microstructure and indentation mechanical properties of plasma sprayed nano-bimodal and conventional ZrO_2—8wt% Y_2O_3 thermal barrier coatings," *Vacuum*, vol. 86, no. 8, pp. 1174–1185, 2012.

[16] X. H. Zheng, H. W. Zhang, X. Huang, N. Hansen, and K. Lu. "Characterisation of micrometre-and nanostructured atmospheric plasma sprayed zirconia—8% yttria thermal barrier coatings," *Materials Science and Technology*, vol. 32, no. 6, pp. 593–601, 2016.

[17] X. Q. Ma, S. Cho, and M. Takemoto, "Acoustic emission source analysis of plasma sprayed thermal barrier coatings during four-point bend tests," *Surface and Coatings Technology*, vol. 139, no. 1, pp. 55–62, 2001.

[18] E. Sadeghi, N. Markocsan, and S. Joshi, "Advances in corrosion-resistant thermal spray coatings for renewable energy power plants. Part I: Effect of composition and microstructure," *J. Therm. Spray. Tech.*, vol. 28, pp. 1749–1788, 2019. https://doi.org/10.1007/s11666-019-00938-1.

[19] A. Keyvani, M. Saremi, and M. H. Sohi, "An investigation on oxidation, hot corrosion and mechanical properties of plasma-sprayed conventional and nanostructured YSZ coatings," *Surface and Coatings Technology*, vol. 206, no. 2–3, pp. 208–216, 2011.

[20] M. H. Habibi and S. M. Guo, "The hot corrosion behavior of plasma sprayed zirconia coatings stabilized with yttria, ceria, and titania in

sodium sulfate and vanadium oxide," *Materials and Corrosion*, vol. 66, no. 3, pp. 270–277, 2015.
[21] R. Goyal, B. S. Sidhu, and V. Chawla, "Investigation of hot corrosion behavior of plasma spray CNTS-aluminum coated ASM-SA213T22(T22) boiler tube steel in actual boiler environment," *International Journal of Latest Trends in Engineering and Technology*, pp. 012–024, 2017.

Copyright © 2024 by the authors. This is an open access article distributed under the Creative Commons Attribution License which permits unrestricted use, distribution, and reproduction in any medium, provided the original work is properly cited (CC BY 4.0).